

## A Tactile Sensing Element for a Whole Body Robot Skin

Takayuki HOSHI, and Hiroyuki SHINODA  
Department of Information Physics and Computing  
The University of Tokyo  
7-3-1, Hongo, Bunkyo-ku, Tokyo, Japan  
{star, shino}@alab.t.u-tokyo.ac.jp

*In this paper, we propose a new tactile sensing element to realize robot skins. The sensing element has a large sensing area (several square centimeters) and acquires not only contact force but also contact area. By arraying the sensing elements, we can cover a large area with a small amount of the sensing elements, and collect rich tactile information. The structure of the sensing element is very simple; two layers of compressible insulators sandwiched between three pieces of stretchable conductive sheets. The structure enables us to obtain the contact force and the contact area from the capacitances between the conductive pieces. We also propose the method to connect the elements to compose the robot skin including no long wires. CMOS LSI sensor/communication chips are arranged at the boundary of the sensing elements, and the chips measure the capacitances between the conductive layers and send signals through the identical conductive layers.*

### 1. INTRODUCTION

Recently, there is a growing interest in home robots that can care for the aged and young children and that can be alternatives to companion animals. In that situation, robots at home are required to be more cautious about surrounding environments than robots at industrial factories because they interact with humans and there are obstacles and unpredictable events around them. To meet this requisite, robot skins which give tactile sensation to the robots are demanded in robotics. The skin is not only a device for the autonomous motion of a robot but also a new form of interface between humans and artificial systems [1].

The major requirements for robot skins are the following.

- They should sensitively detect rich tactile information related to such parameters as shape, pressure, temperature, and so on.
- They should cover large areas such as whole surfaces of robots.
- They should be soft and stretchable to fit robot surfaces and contact humans safely. Softness is also one of important factors to detect touch feelings.

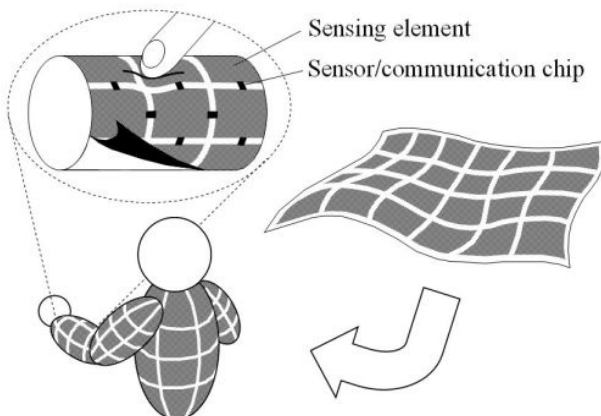


Fig. 1 Tactile sensor skin composed of proposed sensing elements. It is soft, stretchable, and capable to cover a large area easily.

In order to realize such a robot skin, various arrays of tactile sensing elements to detect pressure have been tried [2][3][4]. One approach to enhance the ability of the skins for practical uses is to array the elements in high density. However, we have no practical techniques available now with which we can mount a million of tactile elements with 1 mm spacing in a stretchable sensor skin. We have proposed a new tactile sensing method to solve the problem [5]. In our method, a sensing element has a large sensing area (several square centimeters) and acquires not only contact force but also contact area. Owing to the additional sensing parameter, that is, the contact area, a robot skin which detects minute shape features is easily realized by arraying the elements in low density. In consequence, we can cover whole surfaces of robots with a small amount of the elements (Fig.1). This proposition is inspired by the characteristics of the human tactile sensation. While Two Point Discrimination Thresholds (TPDT) of humans are as large as several centimeters except on especially sensitive areas, the faces and the hands, sharpness of objects can be discriminated sensitively even on such large TPDT parts. From these facts, we suppose that sharpness is one of key components to produce general human tactile sensation [6], and that sensitivity to sharpness is a high priority for human-like sensor skins.

Based on the proposition, we developed a tactile sensing element which acquires not only contact force but also contact area. The sensing element consists of two layers of compressible insulators and three pieces of stretchable conductive sheets. In order to acquire the contact force and the contact area, we make use of the nonlinear elasticity of the insulators. Furthermore, the conductive pieces work not only as sensing elements but also as communication paths when sensor/communication chips are placed at the boundary of the conductive pieces [7]. Thus, wires to sensing elements are no longer needed and stretchable skins can be realized (Fig.2).

In this paper, we describe the structure and the sensing theory of the sensing element [5]. We show experimental

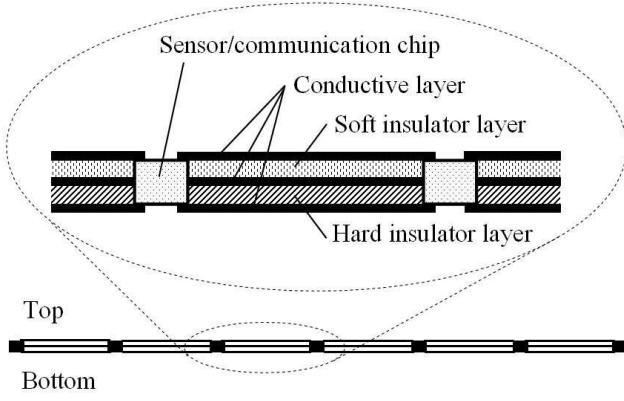


Fig. 2 Cross-section of our robot skin.  
A set of soft and hard layers and three pieces of stretchable conductive sheets form a sensing element.

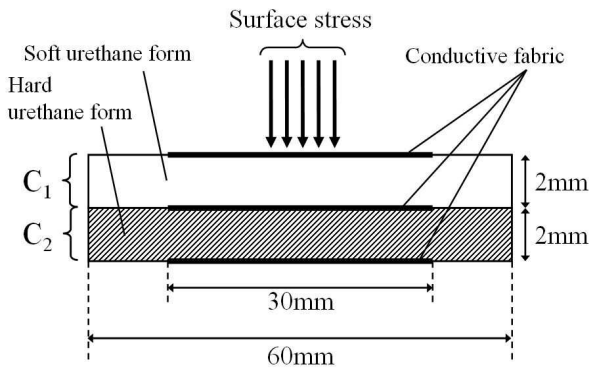


Fig. 3 Cross-section of sensing element prototype.

results to examine the feasibility of the method. We also explain about the communication method using the CMOS LSI sensor/communication chips to eliminate long wires from the sensor skin.

## 2. SENSING ELEMENT

### 2.1 Structure

The structure of our sensing element is very simple. In Fig. 3, we show schematically the cross-section of the sensing element prototype. The sensing element consists of two insulator layers; the upper layer is made of soft urethane foam ( $15 \text{ kg/m}^3$ ) and the lower hard ( $60 \text{ kg/m}^3$ ), and each layer is 2 mm in thickness. There are three pieces of stretchable conductive fabric on the soft layer, between the soft and hard, and under the hard. Each piece has an area of  $30 \times 30 \text{ mm}^2$ . The side length of the conductive fabric piece is comparable to the TPDT on human forearms. The insulator layers and the conductive pieces adhere to each other by soft double-faced tape, and two capacitors are formed in the layers. Supposing a surface of a robot body hard, we attach the bottom of the sensing element prototype to an acrylic base.

### 2.2 Sensing Theory

We suppose a surface stress as illustrated in Fig. 4; a constant surface stress distribution  $\sigma(x, y)$  [Pa] is vertically loaded to the surface of the sensing element in a contact field S, that is,

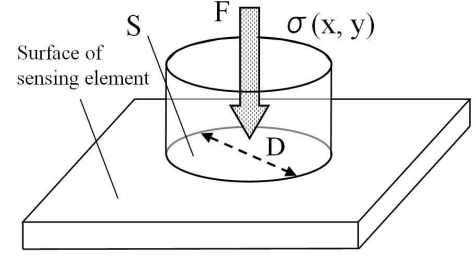


Fig. 4 Supposed surface stress distribution  $\sigma(x, y)$ .

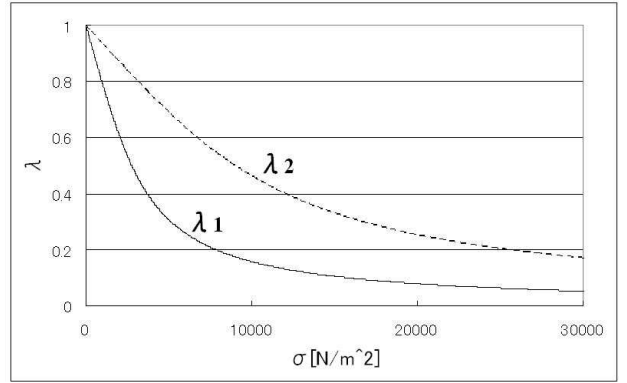


Fig. 5 Relationship between surface stress  $\sigma$  and extension ratio  $\lambda_n$ .  
Soft layer  $\lambda_1$  is more easily compressed than hard layer  $\lambda_2$ .

$$\sigma(x, y) \equiv \begin{cases} F/S & \text{if } (x, y) \in S \\ 0 & \text{if } (x, y) \notin S \end{cases} \quad (1)$$

where  $F$  [N] is the total contact force and  $S$  [ $\text{m}^2$ ] is the area of S. We also assume the following. First, the nonlinear elasticity of the insulator layers is the entropy elasticity [8] expressed as

$$\sigma = \frac{E_n}{3} \left( \frac{1}{\lambda_n} - \lambda_n^2 \right) \quad (n=1, 2) \quad (2)$$

$$\lambda_n \equiv \frac{d_n - \Delta d_n}{d_n} \quad (3)$$

where  $n$  is the layer identification;  $n=1$  means the upper soft layer and 2 the lower hard layer.  $E_n$  [Pa],  $\lambda_n$  and  $d_n$  [m] are the elasticity modulus, the extension ratio and the initial thickness of the layer  $n$ , respectively.  $E_1$  is about 4,750 Pa and  $E_2$  is 15,400 Pa. The following expression of  $\lambda_n$  (Fig. 5) is obtained by solving (2),

$$\lambda_n = \sqrt[3]{\frac{1}{2} + \sqrt{\frac{1}{4} + \left(\frac{\sigma}{E_n}\right)^3}} + \sqrt[3]{\frac{1}{2} - \sqrt{\frac{1}{4} + \left(\frac{\sigma}{E_n}\right)^3}} \quad (4)$$

Second, the conductive pieces have negligible tensions and the Poisson's ratios of the insulator layers are zero, which means that a displacement distribution  $\Delta d_n(x, y)$  [m] is determined simply by the local value of  $\sigma(x, y)$ . We measure electric capacitances  $C_n$  [F] between the conductive pieces to detect  $\Delta d_n(x, y)$ . The capacitances are formulated as

$$C_n = \iint_{\text{Element}} \frac{\epsilon_n}{d_n - \Delta d_n(x, y)} dx dy \quad (5)$$

ignoring fringing fields where  $\epsilon_n$  is the dielectric constant of the layer  $n$ . If we can make the second assumption

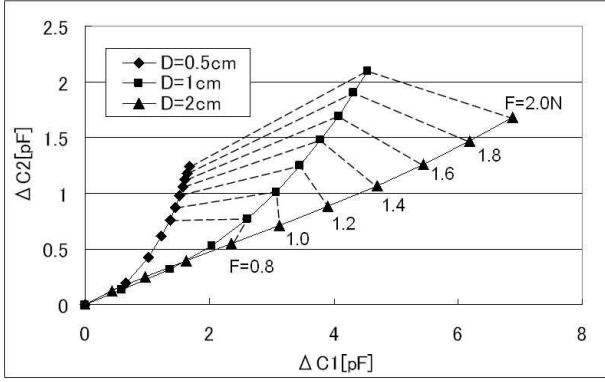


Fig. 6 Simulation result. Calculated  $(\Delta C_1, \Delta C_2)$ s for various  $(F, S)$ s.  $D$  is defined as  $D \equiv 2\sqrt{S/\pi}$  to represent a diameter of  $S$  for a circular object.

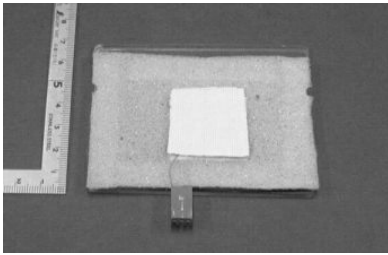


Fig. 7 Photograph of sensing element prototype.

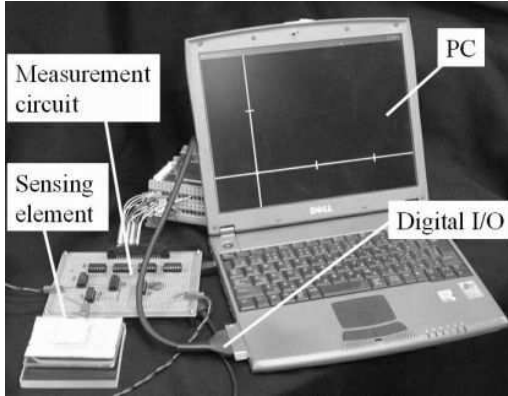


Fig. 8 Experimental setup.

mentioned above,  $(C_1, C_2)$  is uniquely determined by  $(F, S)$ . Then the key question is whether the inverse mapping from  $(C_1, C_2)$  to  $(F, S)$  is possible or not for the layers, 1 and 2, having different hardness.

Fig. 6 shows a numerical simulation result for the elasticity moduli  $E_1 = 4,750$  Pa and  $E_2 = 15,400$  Pa. It shows that  $(\Delta C_1, \Delta C_2)$ s for various  $(F, S)$ s span a two dimensional space, where  $(\Delta C_1, \Delta C_2)$  are the capacitance variation by the applied force, and  $D$  is a parameter defined as

$$D \equiv 2\sqrt{S/\pi} \quad (6)$$

to represent the diameter of  $S$  for a circular object. It implies that we can determine  $(F, S)$  uniquely from  $(\Delta C_1, \Delta C_2)$ .

### 2.3 Experiments and Results

We conducted experiments to examine the feasibility of the proposed sensing method. We measured  $C_n$  of a sensing element prototype (Fig. 7) by a self oscillation method; we

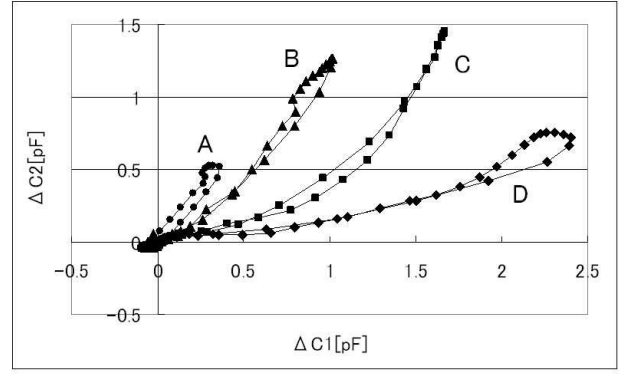


Fig. 9 Experimental result of basic performance. Measured trajectories of  $(\Delta C_1, \Delta C_2)$ s for stimulators A:  $D = 0.5$  mm, B:  $D = 1$  cm, C:  $D = 2$  cm, and D:  $D = 4$  cm.

generated a RC oscillation including the sensing element as the capacitor, and counted pulses per 2 ms by a 16-bit counter. A PC imported data via a digital I/O, and achieved around 80 Hz effective sampling rate (Fig. 8).

#### 2.3.1 Basic Performance

This experiment examined whether the sensing element prototype could discriminate four different stimulators; A:  $D = 0.5$  mm (as an impulse), B:  $D = 1$  cm, C:  $D = 2$  cm, and D:  $D = 4$  cm (as a whole area). Each stimulator was vertically pressed at the center of the sensing element by hand with force up to around 10 N in 0.5 s and it was released after that. In Fig. 9, the  $(\Delta C_1, \Delta C_2)$ s during the motion are plotted. It is confirmed possible to discriminate the four stimulators.

#### 2.3.2 Effect of Surface Configuration

This experiment examined whether the prototype could discriminate the four stimulators A, B, C, and D even when it was placed on the base with the hemispherical bump shown in Fig. 10. As in Section 2.3.1, each stimulator was vertically pressed at the center of the sensing element by hand with force up to around 10 N in 0.5 s and it was released after that. In Fig. 11, the  $(\Delta C_1, \Delta C_2)$ s during the motion are plotted. It is also confirmed possible to discriminate the four stimulators when the sensing element is attached to the curved surface.

#### 2.3.3 Effect of Contact Position

This experiment examined whether the outputs of the prototype had some relationship with the contact position on the surface of the prototype. We pressed the center and the corners of the sensing element as illustrated in Fig. 12 by the stimulator B. We also pressed the center of the sensing element by the stimulators A and C as references. The other conditions were same as the experiment in Section 2.3.1.

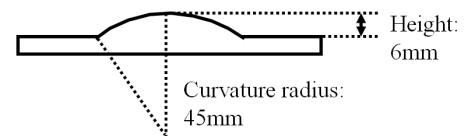


Fig. 10 Base with hemispherical bump.

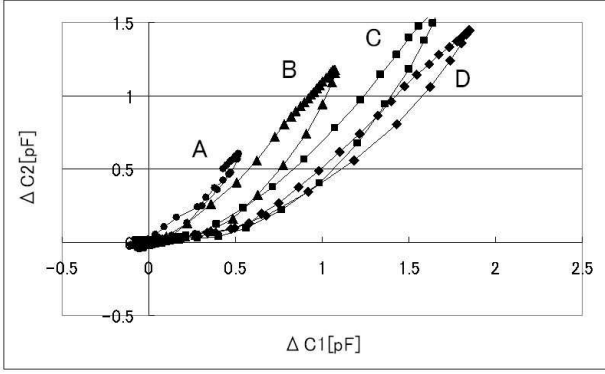


Fig. 11 Experimental result on effect of surface configuration. Measured trajectories of  $(\Delta C_1, \Delta C_2)$ s for stimulators A:  $D = 0.5$  mm, B:  $D = 1$  cm, C:  $D = 2$  cm, and D:  $D = 4$  cm.

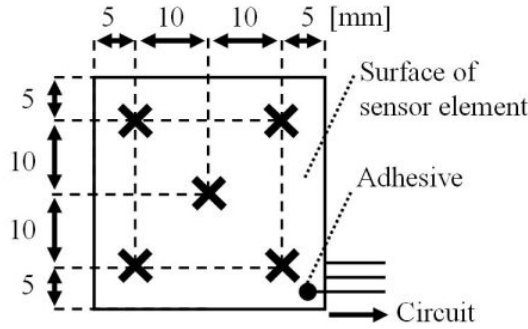


Fig. 12 Pressed positions; the center and the four corners.

In Fig. 13, the  $(\Delta C_1, \Delta C_2)$ s during the motion are plotted. It is confirmed possible to discriminate the stimulator B from the stimulators A and C regardless of the contact positions.

### 2.3.4 Effect of Force Direction

This experiment examined whether the outputs of the prototype had some relationship with the force direction, i.e. the existence of the surface shear stress. We pressed the center of the sensing element by the stimulator A not only vertically but also aslope at an angle of 45 degrees. We also pressed the center by the stimulator B as a reference. The other conditions were same as the experiment in Section 2.3.1.

In Fig. 14, the  $(\Delta C_1, \Delta C_2)$ s during the motion are plotted. It is confirmed possible to discriminate the stimulator A from the stimulator B regardless of the force directions.

### 2.3.5 Reproducibility of Results

This experiment examined whether the outputs of the prototype were reproducible. We used the six stimulators with the diameters  $D = 1.0$  cm, 1.6 cm, 2.0 cm, 2.6 cm, 3.0 cm, and 4.0 cm. Each stimulator was vertically pressed at the center of the sensing element by a mechanical setup measuring the pressing force quasi-statically.

In Fig. 15, the averaged  $(\Delta C_1, \Delta C_2)$ s of the five trials are plotted with the error bars representing the maximal deviations. It is confirmed that the outputs were stable during the five trials.

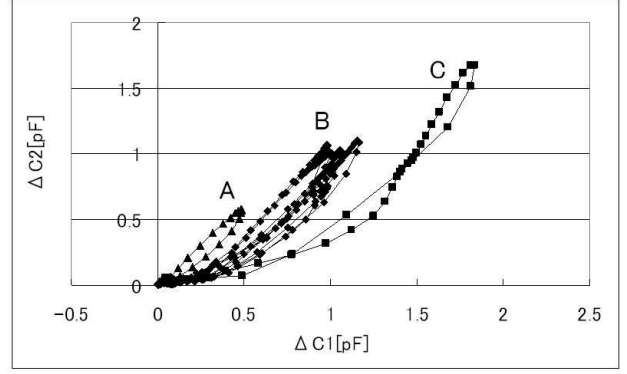


Fig. 13 Experimental result on effect of contact position. Measured trajectories of  $(\Delta C_1, \Delta C_2)$ s for stimulators A:  $D = 0.5$  mm, B:  $D = 1$  cm, and C:  $D = 2$  cm.

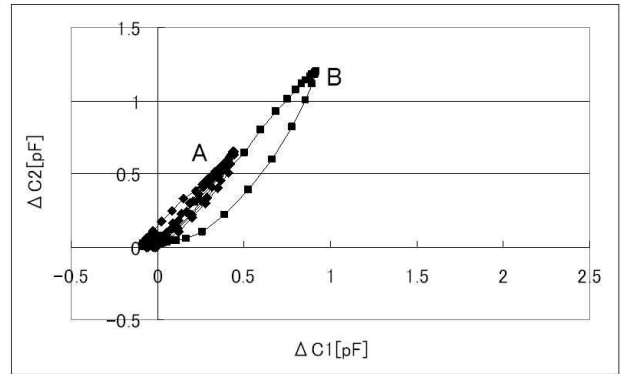


Fig. 14 Experimental result on effect of force direction. Measured trajectories of  $(\Delta C_1, \Delta C_2)$ s for stimulators A:  $D = 0.5$  mm and B:  $D = 1$  cm.

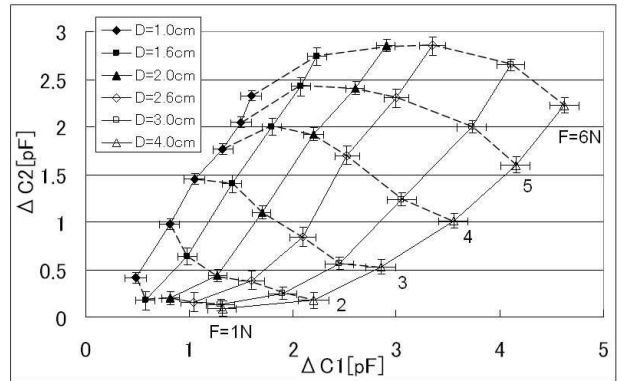


Fig. 15 Experimental result on reproducibility. Averaged trajectories of  $(\Delta C_1, \Delta C_2)$ s for various  $(F, S)$  with error bars representing maximal deviations.

## 3. SENSOR SKIN SYSTEM

### 3.1 Structure

In this research, we are developing a sensing chip that measures the capacitance  $C_n$  and transmits signals to the host computer without long wires. Eliminating long wires is crucial to realize a practical elastic sensor skin. In our method, we also use the conductive pieces of the sensing elements for signal transmission.

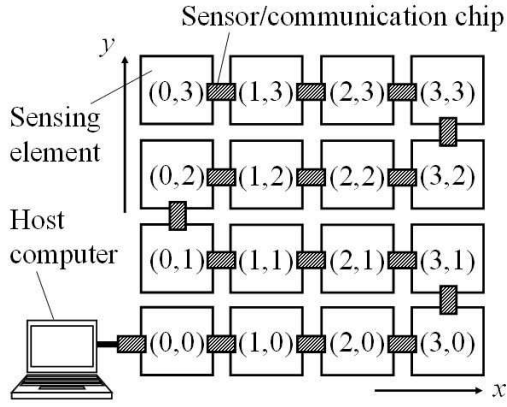


Fig. 16 Scheme of sensor skin. Each sensing element has its specific coordinate as shown in the figure.

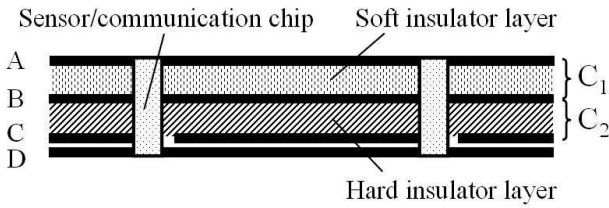


Figure 17. Cross-section of robot skin using current version of LSI chip. A: Ground layer, B: Sensor/signal layer, C: Sensor layer, and D: Power layer.

The scheme of the sensor skin system is illustrated in Fig. 16. The system consists of the arrayed sensing elements and the sensing chips arranged at the boundaries of the sensing elements. Each sensing element has its specific coordinate as shown in Fig. 16. The sensing element with the coordinate (0, 0) is connected to the host computer. While the number of the sensing elements is only 16 in the current version, additional elements could be connected in the same manner.

The cross-section of the sensor skin is shown in Fig. 17. There are four conductive layers; the layers A, B, C, and D are a ground layer, a sensor/signal layer, the other sensor layer, and a power layer, respectively. The sensing chips are supplied power from the power and ground layer. The layers A and B form the capacitance  $C_1$ , and the layers B and C form the capacitance  $C_2$ . The data packets are multi-hopped through the sensor/signal layer to the host computer.

### 3.2 Packets and Operations

In the first version of the protocol, two kinds of packets, the data packet and the command packet are employed. The data packet contains the measured data and the coordinate of the sensing element, and the command packet contains the cue signal for the next chip to measure the capacitances of the sensing element.

Receiving the data packet, the chip transfers the identical packet to the next chip through the signal layer. On the other hand, receiving the command packet, the chip executes the following two-step sequence. Firstly, the chip measures the capacitance  $C_n$  and sends the data packet containing the measured data to the next chip through the signal layer. Next, the chip generates and sends the command packet to

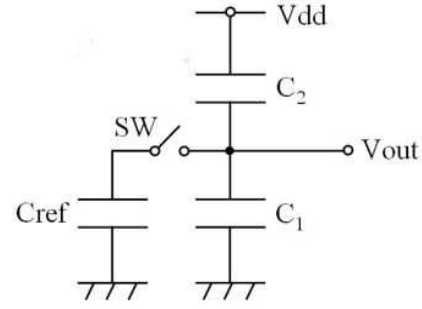


Fig. 18 Equivalent circuit of measurement system.

the next chip. By the iteration of this process, the host computer can gather the data from the all sensing elements. The chip connected to the sensing element with the coordinate (0, 3) alone executes the sequence spontaneously at adequate intervals without waiting for the command packets.

### 3.3 Measurement Method

Fig. 18 shows the equivalent circuit of the measurement system. There is a reference capacitance  $C_{ref}$  inside the chip connected through a switch SW to the junction of the capacitances  $C_1$  and  $C_2$ . The sensing chip measures the divided voltage  $V_{out}$  between the power voltage  $V_{dd}$  and the ground. The divided voltages are represented as

$$V_{out(OFF)} = \frac{C_2}{C_1 + C_2} V_{dd} \quad (7)$$

$$V_{out(ON)} = \frac{C_2}{C_1 + C_2 + C_{ref}} V_{dd} \quad (8)$$

where  $V_{out(OFF)}$  and  $V_{out(ON)}$  mean the voltages of the junction when the switch SW is off and on, respectively. The chip sends the values of  $V_{out(OFF)}$  and  $V_{out(ON)}$  after coding them by an A/D converter on the chip. We can know  $C_1$  and  $C_2$  by solving (7) and (8). The chip has initialization process before the measurement of  $V_{out(OFF)}$  and  $V_{out(ON)}$  in which the charges in  $C_1$ ,  $C_2$  and  $C_{ref}$  are all released.

### 3.4 Prototype of Sensing Chip

At the present stage, we have completed fabrication of the first prototype of CMOS LSI based on 0.35  $\mu\text{m}$  rule for the sensor/communication chip (Fig. 19). The total area of the analog-digital mixed circuits is within 1.5  $\text{mm}^2$ . The operating frequency of the chip is 50 MHz. Each chip measures  $V_{out}$  with an 8-bit A/D converter and it has a function to transmit the data to the neighboring sensing chip. We have verified the chip can measure the capacitances of one sensing element and transmit data to a PC (Fig. 20) successfully. The little finger, the thumb, and the palm of one of the authors were vertically pressed at the center of the sensing element with force up to around 10 N in 0.5 s and they were released after that. In Fig. 21, the  $(\Delta C_1, \Delta C_2)$ s during the motion are plotted. It is confirmed possible to discriminate the three parts of the hand.

We are in the process of arraying the sensing elements using multiple chips.

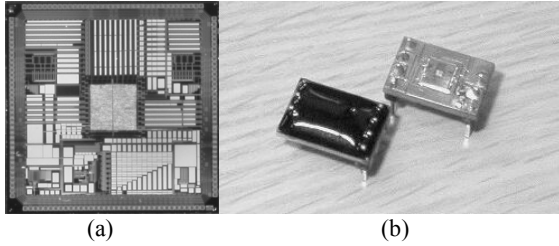


Fig. 19 (a) Closeup top view of current version of CMOS LSI chip. (b) CMOS LSI chip after bonding (right) and molding (left).

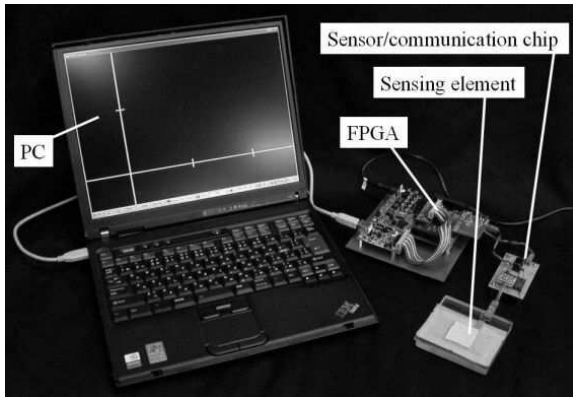


Fig. 20 Examination system using LSI sensor/communication chip.

#### 4. CONCLUSION

In this paper, we proposed a new tactile sensing element using the nonlinear elasticity to acquire not only contact force but also contact area. This sensing method is based on the characteristics of the human tactile sensation. We also introduced a communication method in which the conductive pieces of the sensing elements are also used as the signal transmission layers. By combining these two technologies, we can achieve soft and stretchable robot skins which detect minute shape features of contact objects, and cover whole surfaces of robots.

#### #. ACKNOWLEDGEMENT

We thank Naoya Asamura, Tachio Yuasa, Mitsuhiro Hakozaki, Xinyu Wang, and Hiroto Itai, at Cellcross Co., Ltd. for their cooperation on fabricating and evaluating the prototype of the CMOS LSI chip, and providing ideas on device structures.

#### #. REFERENCES

- [1] M. H. Lee, and H. R. Nicholls: Tactile sensing for mechatronics - a state of the art survey, *Mechatronics*, vol. 9, pp. 1-31, 1999.
- [2] Y. Hoshino, M. Inaba, and H. Inoue: Model and Processing of Whole-body Tactile Sensor Suit for Human-Robot Contact Interaction, *Proc. of the 1998 IEEE International Conference on Robotics & Automation (ICRA '98)*, pp. 2281-2286, 1998.

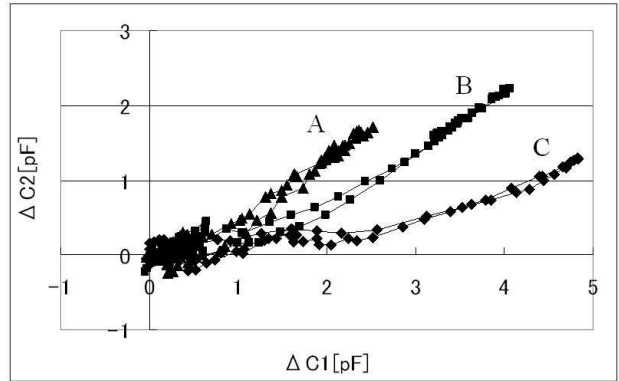


Fig. 21 Experimental result on operation check of first prototype of sensor/communication chip. Measured trajectories of capacitances for stimulators (A) the little finger, (B) the thumb, and (C) the palm.

- [3] R. Kageyama, S. Kagami, M. Inaba, and H. Inoue: Development of Soft and Distributed Tactile Sensors and the Application to a Humanoid Robot, *Proc. of the IEEE International Conference on Systems, Man, and Cybernetics*, vol. 2, pp. 981-986, 1999.
- [4] O. Kerpa, K. Weiss, and H. Worn: Development of a Flexible Tactile Sensor System for a Humanoid Robot, *Proc. of the 2003 IEEE/RSJ International Conference on Intelligent Robots and Systems (IROS 2003)*, vol. 1, pp. 1-6, 2003.
- [5] T. Hoshi, and H. Shinoda: Tactile sensing using nonlinear elasticity, *Proc. of SICE Annual Conference 2005*, pp. 2978-2981, 2005.
- [6] Y. Makino, N. Asamura, and H. Shinoda: Multi Primitive Tactile Display Based on Suction Pressure Control, *Proc. of IEEE 12th Symposium on Haptic Interfaces for Virtual Environment and Teleoperator Systems (Haptic Symposium 2004)*, pp. 90-96, 2004.
- [7] A. Okada, Y. Makino, and H. Shinoda: Cell Bridge: A Signal Transmission Element for Networked Sensing, *Proc. of SICE Annual Conference 2005*, pp. 3826-3831, 2005.
- [8] G. R. Strobl: *The Physics of Polymers: Concepts for Understanding Their Structures and Behavior*, Springer, 1997.